THE ASTROPHYSICAL JOURNAL, 472:891–902, 1996 December 1

INFERENCE OF SOLAR IRRADIANCE VARIABILITY FROM TERRESTRIAL TEMPERATURE CHANGES, 1880–1993: AN ASTROPHYSICAL APPLICATION OF THE SUN-CLIMATE CONNECTION

W. H. SOON,[1,2] E. S. POSMENTIER,[3] AND S. L. BALIUNAS[1,2,4]

Received 1996 February 16; accepted 1996 June 1

ABSTRACT

Information can be inferred on the timing and amplitude of solar total irradiance changes over 1880–1993 by simulating the global terrestrial surface temperature changes produced by these irradiance changes and comparing them with observed temperatures. The profiles of solar irradiance variations used in the climate simulations are adopted from several different proxies: (1) the length of the sunspot cycle, (2) the mean sunspot number, and (3) a composite proxy that includes the two previous indicators plus the equatorial solar rotation rate, the fraction of penumbral spot coverage, and the rate of decay of the sunspot cycle. We use a seasonal energy-conservation climate/upwelling-diffusion ocean model, forced by the assumed profiles of solar total irradiance variations, combined with variations in anthropogenic greenhouse gases. Optimized cases imply total irradiance changes during 1880–1993 in the range 0.18%–0.77%.

If the solar irradiance profiles found from the climate simulations are required to be consistent with recent satellite observations, then the composite solar profile reconstructed by Hoyt & Schatten, combined with the anthropogenic greenhouse forcing, explains the highest fraction of the variance of observed global mean temperatures. In this case, the solar and greenhouse combination accounts for 92% of the observed long-term temperature variance during 1880–1993. The simulation implies that the solar part of the forcing alone would account for 71% of the global mean temperature variance, compared to 51% for the greenhouse gases' part alone. It also suggests a solar total irradiance variation of 0.5% during the interval 1880–1993. Such an amplitude of solar total irradiance change is consistent with astrophysical limits of brightness changes on timescales of decades to centuries independently derived from observations of solar-type stars (including the Sun).

Subject headings: Earth — solar-terrestrial relations — Sun: activity — Sun: fundamental parameters

1. INTRODUCTION

Over the last 4600 million years, the total bolometric luminosity of the Sun should have increased by 30% as the surface temperature readjusted to the increased nuclear energy released in the core (see, e.g., Gough 1988; Gilliland 1989). On shorter timescales, e.g., decades to centuries, surface irradiance changes appear to be governed by or associated with changes in the Sun's surface magnetic activity. Direct satellite measurements of solar total irradiance from 1978 to 1992 indicate an amplitude of variation of $\sim$0.14% during one sunspot cycle, approximately in phase with changes in surface magnetic activity (e.g., Willson & Hudson 1991; Hoyt et al. 1992; Lee et al. 1995). Theory (see, e.g., Gilliland 1982) has yet to account for these decadal changes in brightness or irradiance and their connection with changes in surface magnetism. Other evidence links changes in solar brightness to records of past magnetic activity from the early 17th century to the present (Foukal & Lean 1990; Schatten & Orosz 1990; Hoyt & Schatten 1993; Nesme-Ribes et al. 1993; Lean, Beer, & Bradley 1995).

Hoyt & Schatten (1993) offer an extensive discussion of proxies and models of secular changes in the global solar convective energy and the implied solar total irradiance changes (for detailed studies of energy balance within spatially resolved solar active regions, see also Chapman, Cookson, & Dobias 1994; Steinegger et al. 1996). For example, within the interval from 1880 to 1993, extrapolations based on satellite observations suggest a total irradiance change of at most 0.14% (e.g., Foukal & Lean 1990; Schatten & Orosz 1990).

Another approach to estimating past solar brightness variability depends on an empirical relation between brightness change (as represented by the variation in the Strömgren b and y photometric indices) and surface magnetic activity change (as represented by the net Ca II chromospheric emission) for a group of lower main sequence stars with 30 year records similar to that of the contemporary Sun (e.g., Zhang et al. 1994; Baliunas & Soon 1995). These observations of solar-type stars complement the satellite solar measurements in that they can reveal contributions by other magnetic components (e.g., the active networks) that are presumed missing from the observed solar total irradiance changes during the 1978–1992 interval (e.g., Foukal, Harvey, & Hill 1991; Kuhn & Libbrecht 1991; Willson & Hudson 1991; Soon, Baliunas, & Zhang 1994). Considerations based on brightness and magnetic activity variations of the Sun and a group of solar-type stars yield a bound to the solar irradiance change of 0.2%–0.7% over the past 350 years (e.g., Zhang et al. 1994).

If the Sun's brightness has indeed changed appreciably, i.e., by several tenths of a percent or more on a timescale of decades to centuries, these changes may be discernible through their impact on the global climate records. An

[1] Harvard-Smithsonian Center for Astrophysics, 60 Garden Street, Cambridge, MA 02138.
[2] Mount Wilson Observatory, Mount Wilson, CA 91023.
[3] Science Division, Long Island University, Brooklyn Campus, Brooklyn, NY 11201.
[4] Center for Automated Space Science and Center of Excellence in Information Systems, Tennessee State University, 330 10th Avenue North, Nashville, TN 37203.

examination of the climate record may provide information on the timing and amplitude of solar variability. Such knowledge would be of astrophysical interest.

In order to estimate solar brightness change, we have assumed a combination of solar and greenhouse forcings with time-dependent profiles based on various models of solar variability and from the human buildup of the concentrations of greenhouse gases in the atmosphere. These solar and greenhouse radiative perturbations are incorporated into a global climate model, and their amplitudes are adjusted to secure a best fit of the computed temperature to the observed temperature history of the last 100 years.

The climate model used in this analysis was developed by Posmentier (1994). For the timescales of interest in this analysis, we assumed that the geometrical variation of the Earth-Sun orbital elements on 19, 23, 41, and $\sim$100 kyr timescales (e.g., Laskar, Joutel, & Boudin 1993) may be neglected. A description of the model and its validation by comparison of its results with observed properties are given below and in Appendix A.

With respect to short-term (i.e., interannual) terrestrial climate variability, the theoretical temperature response to annual changes in total irradiance is an order of magnitude smaller than what is observed from 1980 to 1984 (Hoffert, Frei, & Narayanan 1988). Hoffert et al.'s analysis was based on the one-dimensional upwelling-diffusion ocean model of Hoffert, Callegari, & Hsieh (1980). With respect to changes over decades, Hansen et al. (1981) and Gilliland & Schneider (1984) were among the first to consider the transient, interdecadal response of the terrestrial climate to possible long-term total solar irradiance changes. Although including solar forcing in the models improved the fit to the observed temperature, Hansen et al. (1981) argued that only CO_2 and volcanic aerosol radiative forcings contribute significantly to the global temperature changes. (However, their main argument was based on the assumption—now known to be incorrect—that solar total irradiance decreases as sunspot number increases; satellite measurements have shown that the reverse is true.) On the other hand, calculations by Gilliland & Schneider (1984), using a hemispherically resolved version of the energy-balance model, suggested a significant global contribution from solar forcing, which was modeled as a 76 yr periodic variation in total luminosity with 0.3% amplitude.

Later, Reid (1987, 1991) studied the response of sea surface temperature to long-term total solar irradiance variations by using the envelope of sunspot number as proxy (i.e., the 11 yr running mean of the sunspot number, as discussed below). Reid found that a change in total solar irradiance of $\sim$0.6% could explain most of the observed long-term trends (on a timescale of 90–100 yr) in sea surface temperature since 1850. Kelly & Wigley (1992) and Schlesinger & Ramankutty (1992), using two slightly different versions of the energy-balance climate/upwelling-diffusion ocean model, examined the relative contributions of the greenhouse gases, sulfate aerosols, and solar forcings. Both studies showed that the explained variance[5] in global temperature is improved when solar forcing (using the solar cycle length as proxy of brightness change) is combined with the radiative forcing of anthropogenic greenhouse gas emission. For example, the study by Kelly & Wigley (1992) indicated an explained temperature variance of 51% with greenhouse gases' forcing alone and 61% with combined solar and greenhouse effects.

We propose to probe for solar signals in the terrestrial records of global temperature change over the last 100 years at the level of 1% change in solar total irradiance. These cannot be ruled out either by theory (e.g., Gilliland 1982; Endal, Sofia, & Twigg 1985; Arendt 1992; Spruit 1994; Parker 1995) or by observations of the Sun or solar-type stars (e.g., Lockwood et al. 1992; Zhang et al. 1994). Several empirical relations of high statistical significance recently suggested between solar activity (particularly as measured by the length of sunspot activity cycle, P_{cyc}) and terrestrial temperature change can be explained in terms of postulated changes in the solar total irradiance (e.g., Friis-Christensen & Lassen 1991; Hoyt & Schatten 1993; Kim & Huang 1993; Butler & Johnston 1994; Hameed & Gong 1994). We ignore the possibility of additional mechanisms that may induce long-term climate changes (e.g., modulation of tropospheric radiative properties induced by solar UV variability [Haigh 1994; Schatten 1996] or the modification of the global electric circuit and cloud microphysics caused by solar energetic particles [Tinsley, Hoeksema, & Baker 1994]). We shall focus only on perturbations to terrestrial temperature change caused by secular changes in the Sun's total irradiance over the interval 1880–1993.

2. METHOD

2.1. *Description of the Climate Model*

The energy-conservation climate model used in this study resolves seven zones—three in each hemisphere and one intertropical convergence zone (Fig. 1). Each zone is divided into land and ocean areas, with one and two layers, respectively. (The deeper ocean layer is a single layer that includes all seven ocean regions.) The atmosphere in the model consists of two vertical layers (the 1000–500 mbar and $\lesssim$500 mbar layers) in each of the 14 regions. The physical processes accounted for by the model include radiation in three wavelength bands; parameterized evaporation, precipitation, and cloudiness; advection and diffusion in three dimensions; and surface sensible-heat exchange.

The model equations comprise 56 atmospheric equations (heat and water balance, in land and ocean regions, in both layers in each of seven zones), 14 surface heat conservation equations, and one deep-ocean heat conservation equation. The 56 atmospheric equations are steady state. They are solved by iteration for the variables describing an atmosphere in equilibrium with the surface. The warming rates of the 14 regional surface layers and one deep-ocean layer are determined by the heat conservation equations. These are integrated using 256 time steps per year (i.e., the model allows for seasonal changes), resolving the solutions of the 56 atmospheric equations at each time step. A fourth-order Runge-Kutta method is used for the first four steps, after which a fourth-order Adams-Bashforth/Adams-Moulton predictor-corrector method is used. Appendix A describes the model further.

2.2. *Validation of the Energy-Conservation Climate Model*

Table A1 in Appendix A contains a comparison of major climate observables with model results. The model's simu-

[5] The fraction of the variance of observed temperature explained by model simulations is defined as $[1 - \sum (T_{sim} - T_{obs})^2/\mathrm{Var}\ (T_{obs})]$, where Var (T_{obs}) is the variance in observed temperature and T_{sim} and T_{obs} are the model output and observed global average temperatures, respectively.

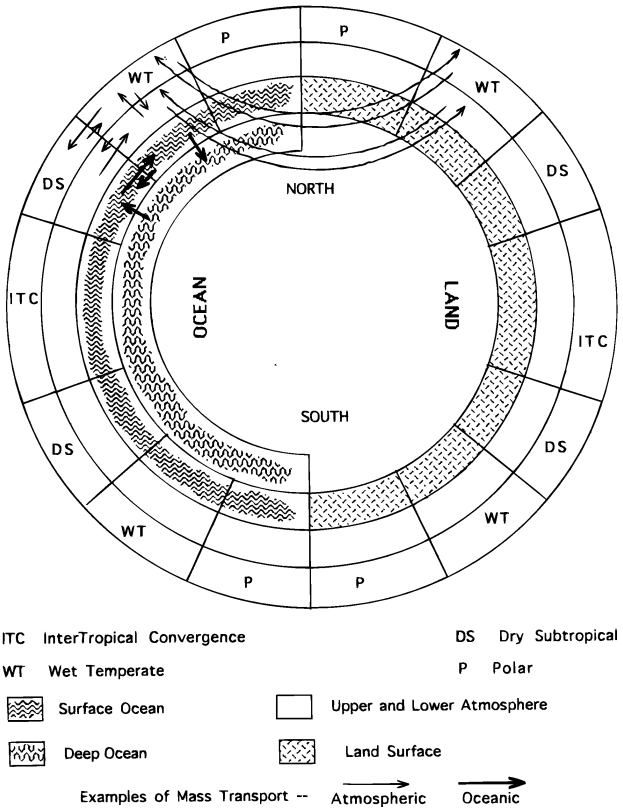

FIG. 1.—Geometry of the energy-balance climate model

lated global, annual average surface temperature of 16.8°C is in reasonable agreement with observations. Diagnostic values of global annual precipitation, snow and ice cover, cloud cover, and energy fluxes also agree quite well with observations. The computed values of the seasonable variation of surface temperature, and of the meridional temperature gradient, are realistic.

Doubling of the CO_2 concentration (with all other variables remaining unchanged) leads to absorption of an additional 4.4 W m^{-2} of back-radiation in the atmosphere, in general agreement with the range of 3.4–4.8 W m^{-2} for CO_2 doubling derived from among 15 general circulation models (GCMs; Cess et al. 1993). The calculated increase in average global temperature for double CO_2 is 1.83°C, compared to warming of 1.5°C–4.5°C suggested by the GCMs (e.g., Cess et al. 1993).

A parallel experiment considers the solar forcing "equivalent" to the CO_2 forcing to be an increase of 4.4 W m^{-2} in the planetary absorption and examines the sensitivity of the modeled climate. Because of differences in individual climate feedback responses between the CO_2 and solar forcing, a warming of 2.33°C results from the "equivalent" solar-forcing calculation. The two results suggest that climate sensitivity via perturbation in solar forcing is about $(2.33-1.83)/1.83 \approx 27\%$ higher than that of CO_2 forcing in our global model. This modeled climate sensitivity of $2.33/4.4 \approx 0.53$°C W^{-1} m^2 is in reasonable agreement with the empirical estimate by Hoyt & Schatten (1993) of 0.7°C W^{-1} m^2 (derived from the NOAA satellites' global terrestrial temperature measurements and *Nimbus* 7's total solar irradiance measurements from 1979 to 1990).

2.3. *Deduction of Time-dependent Forcing Functions*

In the climate simulations, we consider several profiles of reconstructed solar brightness variations: (1) the unsmoothed sunspot cycle length, P_{cyc} (see Appendix B for a discussion of the *measure* of the length of a sunspot cycle)—Waldmeier (1961) covers up to cycle 19; our study extends approximately to the beginning of cycle 23 based on information from the NOAA National Geophysical Data Center's Solar-Geophysical Data reports; (2) the smoothed sunspot P_{cyc} with a low-pass filter of weights 1-2-2-2-1, to emphasize the secular trend of solar activity (e.g., Friis-Christensen & Lassen 1993; Lassen & Friis-Christensen 1995); (3) the envelope of sunspot number based on an 11 year running-mean filter, to emphasize changes from one solar cycle to another (Zhang et al. 1994); (4) other proxies for total irradiance change, including changes in solar equatorial rotation, fraction of penumbral spots, and decay rate of solar cycle, have also been studied by Hoyt & Schatten (1993). Therefore we also consider the composite total irradiance change profile of Hoyt & Schatten (1993), which had been constructed using all five historical indicators of solar total irradiance (see Appendix C for discussion of another useful proxy for long-term solar irradiance changes).

As evidenced by the results of Zhang et al. (1994), the difference in the measured ratios of brightness change to magnetic activity change for a group of solar-type stars suggests an amplitude from as low as ~0.2% to as high as ~0.7% for total solar irradiance changes over 1880–1993. Therefore, we shall consider that all the proposed solar forcing profiles may be multiplied by a stretching factor, a (which is defined as the range of solar brightness change in percent over this interval). The factor a is to be determined by requiring the best fit of the modeled temperature history to the observed temperature.

The time dependence of the anthropogenic CO_2 concentrations is the same as that assumed by the Intergovernmental Panel on Climate Change (see, e.g., Shine et al. 1990; Siegenthaler & Sarmiento 1993; the CO_2 concentration increases from about 290 to 356 ppm between 1880 and 1993). As with solar forcing, the amplitude of greenhouse forcing is adjusted to secure the best fit of the modeled to observed temperatures, either separately or in combination with the solar forcing. The logarithm of CO_2 concentration was multiplied by a stretching factor, b, in order to accomplish the adjustment of greenhouse forcing. In this way, the model implicitly includes response not only to CO_2 but also to other greenhouse gases (see, e.g., Wang, Dudek, & Liang 1992) like methane (CH_4), nitrous oxide (N_2O), and chlorofluorocarbons (CFC-11 and CFC-12). Effects due to aerosols are not considered in these experiments (see discussion in Appendix D).

3. RESULTS AND DISCUSSION

The observational constraint we applied to the simulated climate is based on the record of annual global terrestrial land-air surface temperature from 1880–1993 compiled by Hansen & Lebedeff. Figure 2 compares the record of Hansen & Lebedeff (1987, 1988) to the composite surface averages of land and marine temperature of Parker et al. (1994). Except for the differences prior to 1890, no significant difference exists between the two records. (The two series have a maximum cross-correlation coefficient of 0.88 at zero lag.) We shall not further pursue the issue of "best available global indicator" of Earth surface temperature in

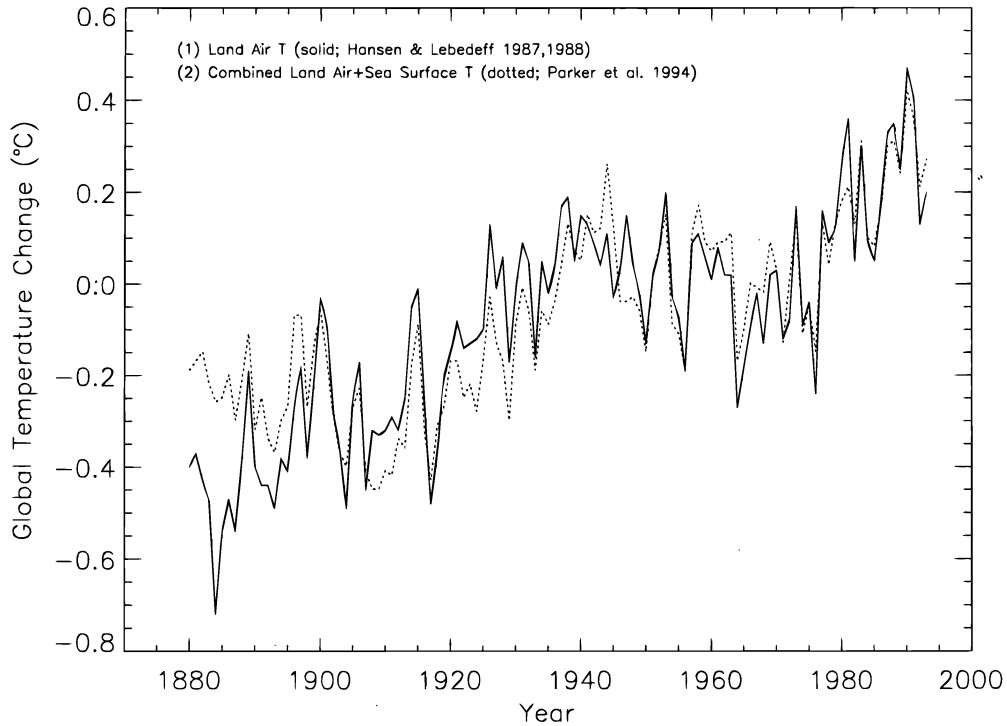

FIG. 2.—Annual average, global land-air surface temperature anomalies (relative to the 1951–1980 reference) derived by Hansen & Lebedeff (1987, 1988; *solid curve*), and the combined land-air and sea surface temperature record of Parker et al. (1994; *dotted curve*). Except for the data prior to 1890, the close concordance of the two reconstructions suggests that the long-term trend of global terrestrial surface temperature changes used in the present study is robust. Spatial coverage of historical temperature series prior to the 1850s to 1860s is poor, and therefore those periods are not considered in this study.

the present study.[6] We smoothed the observed global temperature by an 11 yr running mean in order to remove short-term fluctuations, which are incompatible with the time resolution of the external forcing profiles that we consider. In other words, this study focuses only on the explanations for the long-term (i.e., decades to centuries) trend in the global temperature change record; it does not consider year-to-year variability.

All the time-dependent simulations began by assuming an initial condition with approximately equilibrated atmosphere and ocean since information on the initial conditions is not available. The optimum stretching factors a and b are determined by the best fit between the simulated climates and the smoothed observed temperature record. For each climate run, the fraction of the variance of observed temperature that can be explained by the simulations is computed as a measure of the goodness in the fit.

Figures 3–6 depict the results of the simulations performed in this study. Contours of the fraction of explained variances are presented as functions of the two stretching parameters associated with the solar and greenhouse gases (GHGs) radiative forcings. Table 1 summarizes the information on the optimum fits to the observed temperatures for all radiative-forcing cases, including an intercomparison of the results for the four solar-forcing profiles. Table 1 also shows that the highest explained variance arises consistently out of cases that have considered the combined effects of anthropogenic greenhouse gases and solar radiative forcings. Figure 7 shows the best simulated temperature changes over 1885–1897 for the combined GHG and Sun and the separate contributions by the GHG and solar forcings. The rest of the discussion describes experiments for GHG and solar forcings alone and then the results with combined forcings.

3.1. *Greenhouse Forcing Alone*

The GHG-only solution (case 1 in Table 1) ignores the radiative contribution induced by the postulated changes in external solar total irradiance to the global temperature changes. A scaling in concentration of CO_2 from 354 to 660 ppm was required by the climate equilibrium GCM experiments of Wang et al. (1992) to equate the increase in radiative forcings (a differential increase of ~ 3.1 W m^{-2} in the troposphere-surface system) induced by the other GHGs to that of CO_2 alone. Wang et al.'s scaling is equivalent to using a stretching factor b of 1.86, in excellent agreement with our optimum value of 1.8.

The simulated temperature changes over the 1885–1987 interval account for 63% of the observed temperature variance, and the maximum value of 0.55°C compares well with the observed maximum change of 0.72°C. Because of the monotonic increase in the CO_2 profile, the combined GHG forcing fits only the part of the increasing observed temperature changes since the 1970s. From results presented in Figures 3–6, or the optimized radiative forcings in Table 1, we find that, except for the case of reconstructing solar total irradiance by the smoothed sunspot numbers (e.g., cases C2–C4 in Table 1), the addition of a solar component considerably increases the explained percentage of the observed global temperature variance. Therefore, an explanation of global temperature anomalies entirely by the radiative forcing of anthropogenic GHG alone is not optimal.

[6] The NOAA satellite temperature record covering 1979 to the present (see, e.g., Christy 1995) remains too short to be applied in the present study of variability on timescales of decades to centuries.

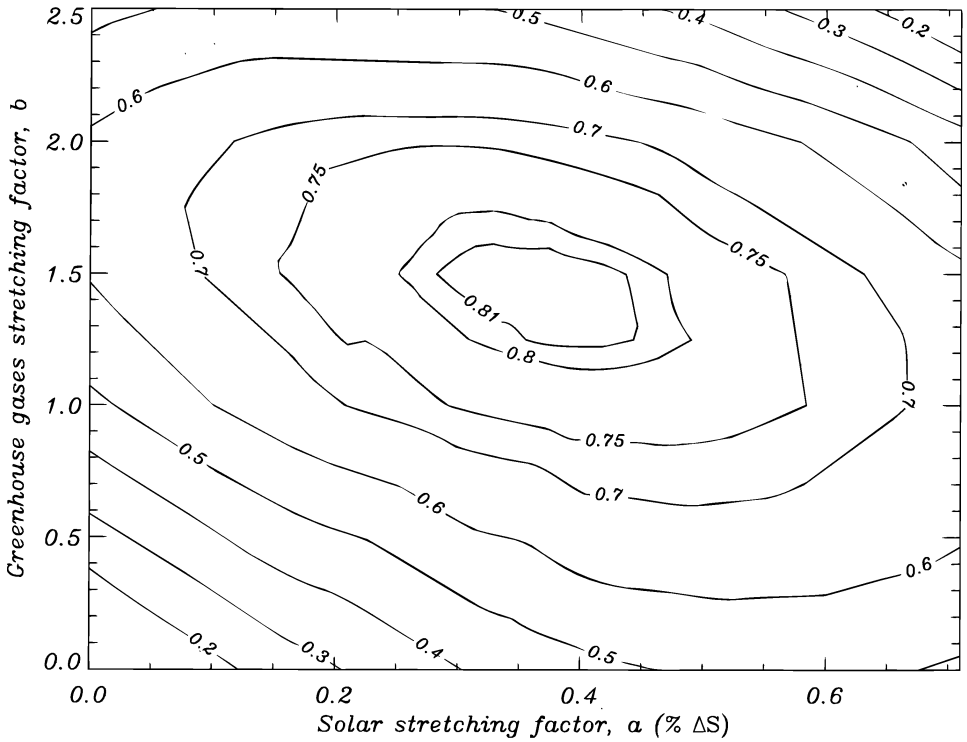

FIG. 3.—Contours of the fraction of explained global temperature variance (1885–1987) as functions of the solar stretching factor, a, and the GHG stretching factor, b. The original solar total irradiance profile (before stretching) is reconstructed from the unsmoothed sunspot activity cycle, P_{cyc} (Waldmeier 1961). See Table 1 for additional results.

3.2. *Solar Forcing Alone*

We consider the radiative-forcing case to estimate the *upper bound* on the solar total irradiance changes, especially for the early portion of the temperature record. The solutions optimized to the global temperature changes rule out a total solar irradiance change greater than 1.0% during the 1880–1993 interval (see also, e.g., Crowley & Kim 1996). The results for the four solar forcing profiles in Table 1

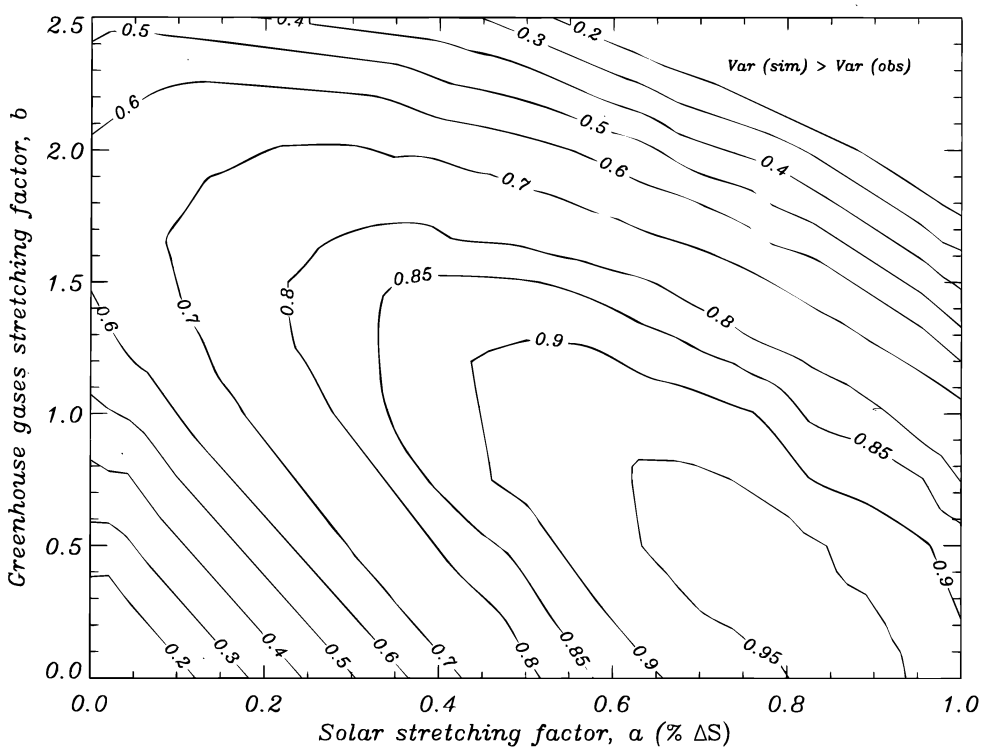

FIG. 4.—Same as Fig. 3, but for the original solar total irradiance profile reconstructed from the smoothed sunspot activity cycle, P_{cyc}; adopted from Friis-Christensen & Lassen (1993). See Table 1 for additional results.

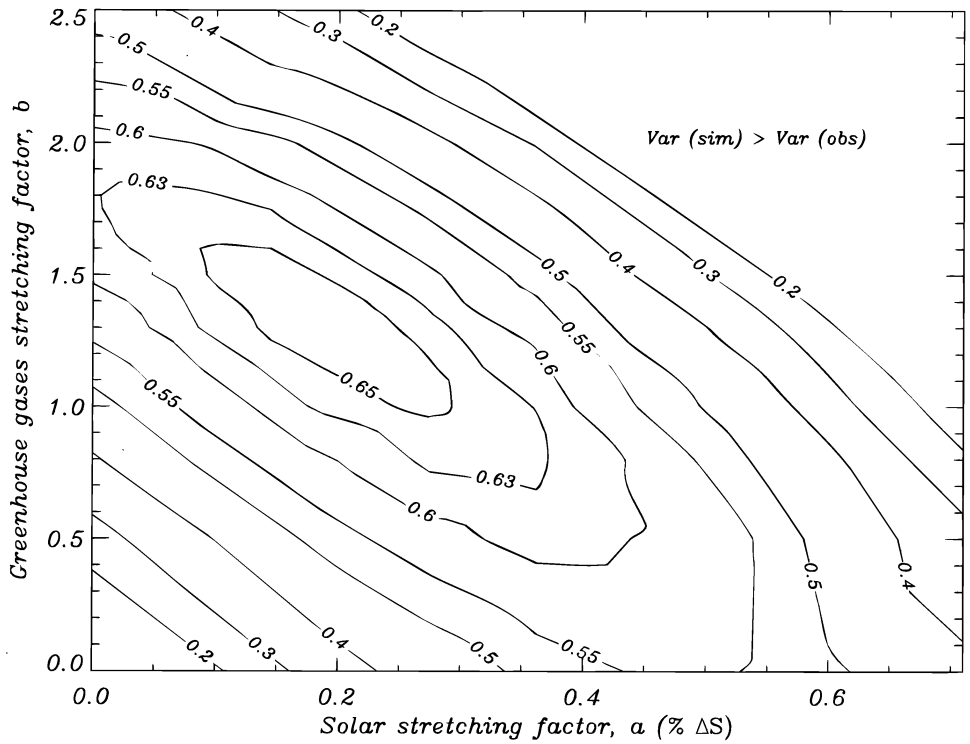

FIG. 5.—Same as Fig. 3, but for the original solar total irradiance profile reconstructed from the 11 yr running mean of sunspot number; adopted from the results of Zhang et al. (1994). See Table 1 for additional results.

indicate that over 50% of the observed temperature variance (which corresponds to over ≈ 0.4°C of global temperture change) can be explained by changes in the Sun's total irradiance alone. However, the best-fit temperature change is sensitive to the filtering scheme applied to the solar profile. For example, the primary difference between the optimized unfiltered (A2) and filtered (B2) profiles based on the length of the sunspot activity cycle arises from the 1970–1990 interval. The implied solar total irradiance change derived from the smoothed sunspot profile (case B2 in Table 1) successfully accounts for nearly the entire variance (96%!) of the observed temperature change but is a

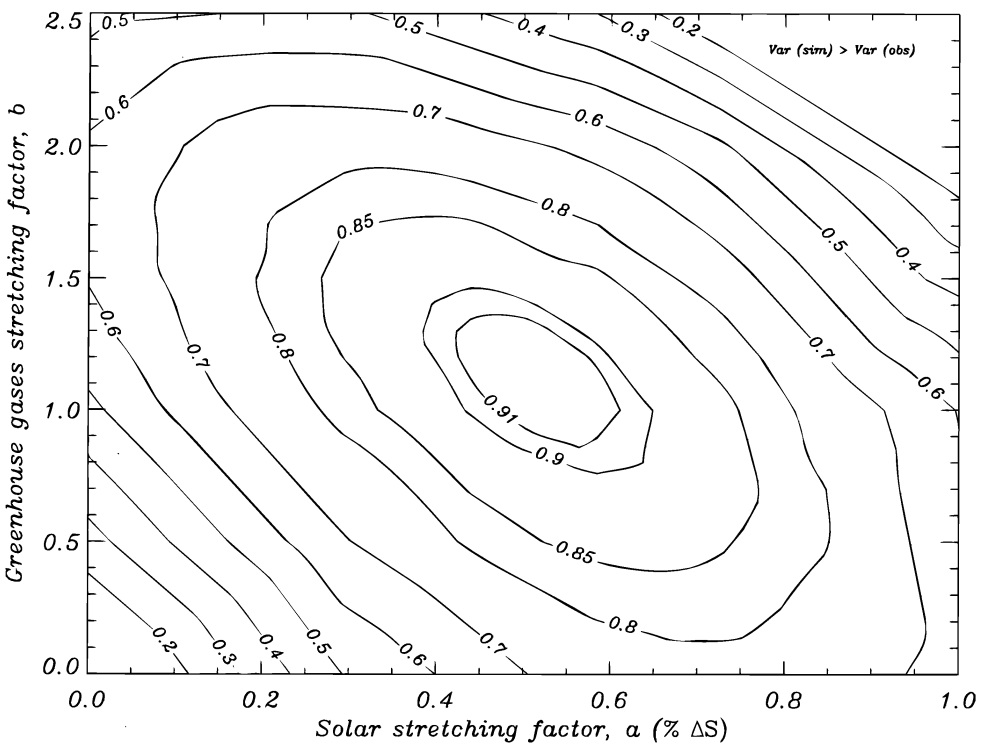

FIG. 6.—Same as Fig. 3, but for the original solar total irradiance profile from the composite total solar irradiance suggested by Hoyt & Schatten (1993). See Table 1 for additional results.

TABLE 1

BEST-FIT OF GLOBAL TERRESTRIAL SURFACE TEMPERATURE CHANGES, 1885–1987

FORCING	STRETCHING FACTORS		EXPLAINED VARIANCE (%)	ΔT_{max} (model) (°C)
	Solar	GHG		
Unsmoothed Sunspot P_{cyc} Profile (Waldmeier 1961)				
Case 1: GHG alone	...	1.8	63	0.55
Case A2: Sun alone	0.58	...	52	0.47
Case A3:				
GHG plus Sun	0.37	1.5	82	0.72
GHG contribution.....	...	1.5	61	0.44
Sun contribution.....	0.37	...	46	0.30
Case A4:				
CO_2 plus Sun	0.44	1.0	78	0.61
CO_2 contribution	...	1.0	47	0.27
Sun contribution.....	0.44	...	49	0.27
Smoothed Sunspot P_{cyc} Profile (Friis-Christensen & Lassen 1993)				
Case 1: GHG alone	...	1.8	63	0.55
Case B2: Sun alone	0.90	...	96	0.70
Case B3:				
GHG plus Sun	0.77	0.5	96	0.74
GHG contribution.....	...	0.5	26	0.13
Sun contribution.....	0.77	...	94	0.60
Case B4:				
CO_2 plus Sun	0.58	1.0	94	0.74
CO_2 contribution	...	1.0	47	0.27
Sun contribution.....	0.58	...	85	0.45
Sunspot Number Envelope Profile (Zhang et al. 1994)				
Case 1: GHG alone	...	1.8	63	0.55
Case C2: Sun alone	0.47	...	56	0.39
Case C3:				
GHG plus Sun	0.18	1.3	66	0.52
GHG contribution.....	...	1.3	57	0.37
Sun contribution.....	0.18	...	34	0.15
Case C4:				
CO_2 plus Sun	0.27	1.0	65	0.49
CO_2 contribution	...	1.0	47	0.27
Sun contribution.....	0.27	...	45	0.22
Composite Total Solar Irradiance Profile (Hoyt & Schatten 1993)				
Case 1: GHG alone	...	1.8	63	0.55
Case D2: Sun alone	0.72	...	78	0.57
Case D3:				
GHG plus Sun	0.52	1.1	92	0.64
GHG contribution.....	...	1.1	51	0.31
Sun contribution.....	0.52	...	71	0.41
Case D4:				
CO_2 plus Sun	0.55	1.0	92	0.63
CO_2 contribution	...	1.0	47	0.27
Sun contribution.....	0.55	...	73	0.43

NOTES.—Case 1: Best-fit GHG forcing (no solar forcing). Cases A2–D2: Best-fit solar forcing (no GHG forcing). Cases A3–D3: Best-fit combination of both forcings. Cases A4–D4: Best-fit solar forcing with GHG stretching factor fixed at 1.0.

The solar stretching factor is the maximum total irradiance change (ΔS, in percent) between 1885 and 1987, after stretching. A GHG stretching factor of 1.0 is equivalent to 1 unit of CO_2 contribution (see, e.g., Siegenthaler & Sarmiento 1993). Explained variance is the percentage of the observed 11 yr moving-averaged global land temperature variance of Hansen & Lebedeff (1987, 1988) explained by the best-fit climate simulation. Model ΔT_{max} may be compared with the observed value of 0.72°C.

factor of ~4–5 higher than the relative bound of 0.14% provided by the *Nimbus-7* satellite measurements over much of the same interval. Therefore, the optimized solution B2 may be ruled out by the satellite measurements. On the other hand, the relative optimized solar irradiance changes based on the unsmoothed P_{cyc} profile (case A2), the mean sunspot number (case C2), and the composite profile of Hoyt & Schatten (1993; case D2) are within the limit imposed by the satellite data since 1978.

The three distinct upper bounds (with maximum relative brightness change of 0.58%, 0.47%, and 0.72% for cases A2, C2, and D2, respectively) constrained by global temperature changes compare well with the upper bound of 0.7% independently derived from the mean sunspot numbers and the empirical activity and brightness-change relation of Zhang et al. (1994). An attempt to identify the best solar profile from the most probable radiative-forcing case of the combined GHG and solar contributions is described below.

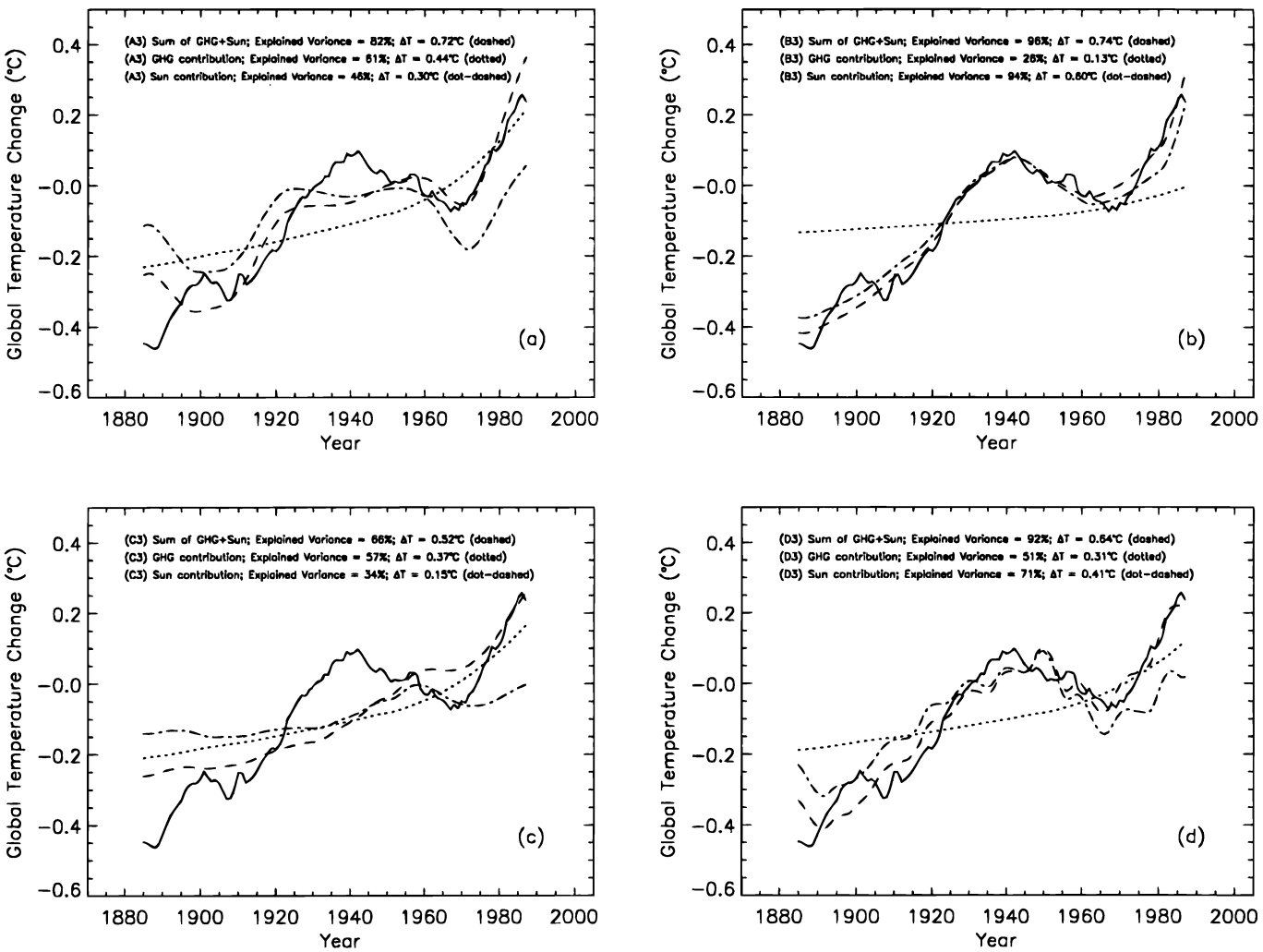

FIG. 7.—Optimum fits to the observed global temperature variations for the combined GHG-plus-Sun forcings (case 3 of radiative forcings in Table 1). The solid curve is the 11 yr running mean of the observed global temperature anomalies from Hansen & Lebedeff (1987, 1988), and the dashed curve is the best simulated global temperature changes. Dotted and dot-dashed curves show separate contributions by GHG and solar radiative forcings to the sum of the best fits, respectively. The four different panels present the four solar forcing profiles. The composite total irradiance profile derived by Hoyt & Schatten (1993) in (*d*) may be the most probable solar total irradiance profile (see text).

3.3. *Combined Greenhouse and Solar Forcings*

The introduction of a second factor to either of the forcing experiments of GHG alone or solar alone leads to a reduced role for each forcing. The optimum GHG stretching factor b is now between 0.5 and 1.5 (instead of 1.8), while the solar stretching factor a is reduced to 0.18 (case C3), 0.37 (case A3), 0.52 (case D3), and 0.77 (case B3). The optimum combination of the two external factors in those cases produces *at least* 65% of the observed global temperature variance (Table 1).

Except for the solar forcing profile derived from the smoothed variations in sunspot cycle lengths (case B3), all the combined GHG and solar cases yield best fits that imply a greenhouse stretching factor greater than that of CO_2 forcing alone. As noted above, the contribution from the GHG forcing is noticeable from 1970 onward. These two remarks taken together suggest that the radiative forcing induced by anthropogenic GHG, has become nonnegligible since the 1970s in our model.

Next, one could ask if any of the optimized solar forcing profiles is preferable. It should again be emphasized that the amplitude of solar brightness changes, as suggested by the optimized solutions, is in fact *not* inconsistent with the empirical results derived from observations of solar-type stars (Lockwood et al. 1992; Zhang et al. 1994). If one were to invoke the irradiance constraint provided by the satellite observations, as in the case of solar forcing alone, then the possibility of solar forcing in B3 can be ruled out. If preference were to be based on the highest possible explained variance, then D3 is clearly the most probable solution of the remaining three. This optimized result obtained with composite solar forcing of Hoyt & Schatten (1993) accounts for 92% of the observed variance (see also Fig. 7*d*).

In addition to the two-parameter best-fit solutions, we have also found the optimized results subject to the constraint that GHG radiative forcing results only from CO_2 (i.e., $b = 1.0$) in Table 1, case 4. The least difference between the best-fit results for cases 3 and 4 occurs with the solar forcing profile D. The results for simulations D3 and D4, and the comparison between D2 and 1, all support the contention that solar radiative forcing has contributed at least as much as GHG to global temperature changes since 1880. A firmer physical basis for distinguishing those optimized histories of solar brightness variations in Table 1

should be possible from a detailed solar spectral irradiance reconstruction at all wavelengths (e.g., by using historical Ca II K spectroheliograms in the interval 1920–1960), such as that initiated by Fontenla et al. (1995).

Finally, we present the following standard multiple regression analysis. Since three time series (solar, CO_2, and observed temperature) are considered in our multivariable fits, this first type of information has statistics with $K - 1 = 2$ degrees of freedom. The temperature record contains a total of 114 annual points. Applying the 11 yr running-mean filter reduces N to ~ 10, so the second type of information has statistics with $N - K = 7$ degrees of freedom. For case D3, whose explained variance is 92%, we computed an F-value of

$$\frac{R^2}{(1 - R^2)} \frac{(N - K)}{(K - 1)} = \frac{0.92}{(1 - 0.92)} \frac{(10 - 3)}{(3 - 1)} = 40.25 ,$$

where R is the multiple-correlation coefficient (see, e.g., Bevington & Robinson 1992). Since the 99th percentile of the $F(2, 7)$ distribution is 9.55, one can reject the null hypothesis that the observed global temperature anomalies and the simulated temperatures (computed from the stretched Hoyt-Schatten solar forcing and anthropogenic CO_2 forcing profiles) are samples of unrelated time series.

The statistical significance of the differences between the explained variance in case D3 (92%) and in cases A3 and C3 (82% and 66%, respectively) may also be evaluated. Applying Fisher's z-transformation to R in each case, and taking $1/[(N - 3) - (K - 2)]^{1/2} = 1/\sqrt{6}$ as the standard deviation of a normally distributed z-variable, we find that the fit for case D3 differs from fits for cases A3 and C3 with the two-tailed significances of 71% and 95%, respectively. Thus the explained variance from the fit by Hoyt & Schatten (case D3) profile is significantly better than Zhang et al.'s (case C3) and may be better than Waldmeier's (case A3).

4. ADDITIONAL COMMENTS

The constraint on total solar irradiance change over 1880–1993 provided by the global surface temperature record is an additional way of obtaining information on solar irradiance change, distinct from direct irradiance measurements and results of solar-type stars. We have viewed the variations in climate as a passive system responding to changes in external radiative forcings. Internal climate variability due to the nonlinear interactions among the climate variables could serve as an alternate explanation to the observed global temperature changes over the same interval (see, e.g., Hasselmann 1976; Gaffin, Hoffert, & Volk 1986; Lorenz 1990; Posmentier 1990; Ghil 1991). However, the high probability of past solar total irradiance changes (as represented by the total irradiance profile reconstructed by Hoyt & Schatten 1993 and as constrained by the empirical relation between brightness and magnetic activity changes derived from measurements of solar-type stars by Zhang et al. 1994) may qualify solution D3 as the simplest physical explanation yet known for the observed long-term changes in the global surface temperature over 1880–1993.

We thank Douglas Hoyt for the composite solar total irradiance profile and Matthew O'Donnell and David Parker (with the help of Michael Schlesinger) for the combined land-air and sea surface, global temperature anomalies applied in this research. Eugene Avrett, Jose Luis Ballester, and Jacques Laskar have also kindly communicated the results of their research to us. Finally, we acknowledge the dedicated efforts of our colleagues at Mount Wilson Observatory. W. H. S. would also like to thank Eugene Avrett for his constant encouragement. Thanks are extended to the two referees—Ronald Gilliland, the other anonymous—for their comments.

This program was supported by the Electric Power Research Institute, Mobil Foundation, Inc., Texaco Foundation, Inc., Scholarly Studies Program, and Langley-Abbot Fund of the Smithsonian Institution, American Petroleum Institute, and Richard C. Lounsbery Foundation. This research was made possible by a collaborative agreement between the Carnegie Institution of Washington and the Mount Wilson Institute.

APPENDIX A

DETAILED DESCRIPTION OF THE CLIMATE MODEL

The three bands considered in the radiative fluxes are: (1) solar, (2) terrestrial radiation in black and nearly black parts of the spectrum, and (3) terrestrial radiation in other parts of the spectrum. Each layer of the atmosphere may absorb, backscatter, or transmit radiation. The coefficients, which are constrained by published observations, depend on the band, the layer, and the presence or absence of clouds. The net radiation balance of each layer in each region is taken to be the area-weighted average of the balances in the parts of the region with no clouds, low-layer clouds only, high-layer clouds only, or both types of clouds.

Meridional and zonal mean winds based on Peixoto & Oort (1992), and vertical winds computed to satisfy continuity, were used to determine the advection of both heat and water vapor among atmospheric cells. The advective effects of symmetric-winds back and forth between adjacent cells, representing diffusive processes, incremented the advection due to the mean winds. During preliminary experiments, the winds were adjusted to provide the best agreement with observed meridional temperature gradients and with interzonal differences in cloudiness and were held constant in all subsequent experiments. Sinking of surface water at high latitudes was assumed to be proportional to the surface area of the ocean poleward of the freezing isotherm. Continuity determines the meridional surface velocities and upwelling in both layers. Similarly, the advective effects of symmetric ocean currents back and forth between adjacent cells, representing diffusive processes, incremented the advection due to the meridional currents. During preliminary experiments, the constant of proportionality for high-latitude sinking, and the diffusive currents, were adjusted to provide the best agreement with observed meridional temperature gradients, and were held constant in all subsequent experiments.

TABLE A1

REFERENCE CLIMATE: COMPARISON OF ANNUALLY AVERAGED MODEL REFERENCE CONDITIONS WITH OBSERVED CONDITIONS

Parameter	Model	Observed
SURFACE TEMPERATURE[a]		
T (°C):		
Global	16.8	14 to 17
North polar	−8.6	−18 to −5
Northern wet temperate	7.2	−5 to 13
Northern dry subtropical	25.9	13 to 29
Intertropical convergence	21.9	24 to 29
Southern dry subtropical	26.7	13 to 29
Southern wet temperate	11.1	−5 to 13
South polar	−2.4	−18 to −5
Hydrologic Cycle[b]		
Precipitation (mm yr^{-1})	996	973
Snow and ice area (%)	12.3	12
Cloud area (%)	33	...
Energy Fluxes[c]		
Solar radiation (%):		
Absorbed in atmosphere	17.4	20
Absorbed at surface	50.3	50
Planetary albedo	32.3	30
Terrestrial radiation (%):		
Back-radiation	118.9	115
Absorbed in atmosphere	113.5	109
Transmitted to space	5.4	6
Counterradiation	97.0	95
Radiation budget (%):		
Latent	23.3	24
Sensible	5.2	6
Deep Ocean[d]		
Temperature (°C)	2.83	3 to 4[e]
Downwelling volumetric flow rate (10^6 m^3 s^{-1})	26	45 ± 10
Upwelling velocity (m yr^{-1})	2.2	4

[a] Observed values are approximate ranges estimated from Lindzen & Farrell 1980 and Stone & Risbey 1990.
[b] Observed values based on Peixoto & Oort 1992.
[c] Model values are percentages of 339 W m^{-2}; observed values are percentages of 345 W m^{-2} from Peixoto & Oort 1992.
[d] Observed values based on Hoffert et al. 1980.
[e] In the 1000–2000 m layer.

Evaporation from the sea surface was assumed to be proportional to the difference between the vapor pressure of the sea surface and that of the lower layer of air. On land, the proportionality was set to half that on the ocean, but evaporation was not permitted to exceed the regional precipitation. The function used to represent cloud cover as a function of humidity in each layer was assumed to be a smoothed step rising from 0% to 43% when the respective layer reaches saturation. Similarly, a function that is a smoothed step rising from zero to one when the respective layer reaches saturation was multiplied by the water vapor in excess of saturation to determine the amount of precipitation. The values of the constants were adjusted to obtain the best fit with observed global and interzonal variations of precipitation and cloudiness, prior to the experiments reported here.

The upward surface flux of sensible heat was assumed to rise exponentially with surface-air temperature difference for small differences and more slowly for very large differences. The parameters used were adjusted to yield the best fit with sensible-heat flux observations.

Table A1 compares the equilibrium (i.e., with time-independent external solar and GHG forcings) results of our climate calculation to the observed mean conditions.

APPENDIX B

LENGTH OF THE SUNSPOT CYCLES

We define the length of the sunspot cycle, P_{cyc}, as the separation between two consecutive minima. The date of each cycle is the time of cycle maximum. Since the length between two consecutive cycles is conserved, the imprecision of determining the timing of each cycle length measured in this way introduces error only in a random sense. (The phase shift of the consecutive

sunspot cycle performs essentially a random walk, except for the hint of a phase maintenance from cycles 1 to 5 [Bracewell 1988; Dicke 1988; see also, e.g., Hoyt & Schatten 1992 for additional sunspot information obtained from about cycles 3–5 and Gough 1990 and Hoyng 1993 for additional discussion on temporal coherency of the solar cycle]). We consider the record of unsmoothed P_{cyc}-values in order to assess the sensitivity of climate results on the random fluctuation introduced by the potential error in timing. This result should be compared to that obtained by using the sunspot P_{cyc} profile that has been filtered by using the low-pass 1-2-2-2-1 filter, as emphasized earlier, by Gleissberg (1944). Alternatively, Hoyt & Schatten (1993) measured the cycle length as the time elapsed between two points with equal normalized activity level from one activity cycle to another. In adopting such a measure, each annually averaged sunspot number is utilized. The activity-cycle length profile produced by that technique is not significantly different from the cycle profile smoothed by the low-pass binomial filter. Also note that, after 1850, another measure of the activity cycle's length, which uses consecutive sunspot maxima, does not produce a significantly different time profile of long-term solar activity.

APPENDIX C

ANOTHER PROXY OF SOLAR TOTAL IRRADIANCE

For completeness, we describe another potential indicator of solar total irradiance change: the degree of symmetry between the coverage of magnetically active regions (e.g., areas of dark sunspots) about the solar equator from one cycle to another. The distribution of solar activity (particularly magnetic elements, such as dark sunspots and bright faculae) on the surface of the Sun exhibits north-south asymmetry (see e.g., Tang, Howard, & Adkins 1984; Swinson, Koyama, & Saito 1986; Antonucci, Hoeksema, & Scherrer 1990; Vizoso & Ballester 1990; Yi 1992). During the Maunder-minimum interval, for example, not only was the number of spots reduced, but the degree of north-south asymmetry was also at its extreme; sunspots almost completely disappeared from the northern solar hemisphere (Ribes & Nesme-Ribes 1993). Verma (1993) has computed a north-south asymmetry index using a wide range of solar magnetic phenomenon (including sunspot area) since solar cycle 8 and suggested that the asymmetry indices may have a long-term trend with characteristic timescale of about 110 years, noted earlier by Waldmeier (1957, 1971). That long-term trend in the asymmetry of spottedness, which adds to hints of secular modulation of solar total irradiance, is related to the slow shift from dominant asymmetry in the north for cycles 8–9 (circa 1834–1856) to south-dominant asymmetry for cycles 10–13 (circa 1856–1902) and the continual north-dominant spot coverage for cycles 14–21 (circa 1902–1987). Oliver & Ballester's (1994) statistical analysis supports the long-term trend for north-south asymmetry in sunspot areas, and they have added that the dominance of northern activity of the last century has been shifting south during the current cycle 22.

APPENDIX D

FORCING DUE TO SULFATE AEROSOLS

The radiative forcing induced by sulfate aerosols is yet another anthropogenic agent that might complicate the analysis of contemporary climate (Charlson et al. 1992; Kiehl & Briegleb 1993; Taylor & Penner 1994). In contrast to greenhouses gases, both the direct (backscattering of solar radiation by the submicron- to micron-size sulfate aerosol particles; see, e.g., Cox, Wang, & Schwartz 1995) and indirect (a hypothesized, enhanced cloud albedo due to increased cloud droplet numbers; see, e.g., Erickson, Oglesby, & Marshall 1995) consequences of increased concentration of sulphate aerosols in the atmosphere is the tendency to cool the global temperature. For the direct effect, Cox et al.'s (1995) GCM simulations suggested a climate sensitivity of the order of 1.25°C W^{-1} m^2, an approximately equal but opposite effect to CO_2 forcing. However, a key distinction between aerosols and GHGs is the inhomogeneous nature (both in latitudinal and vertical extents) of the sulfate aerosols' forcing, in which, according to the example of simulation results by Cox et al. (1995), the uneven aerosol loading tends to cool the Northern Hemisphere's temperature while a southern warming is predicted. In our simplified view of Earth's climate and the focus on long-term global energy balance of the solar-terrestrial system, we shall assume that the equilibrium response of climate perturbation due to combined anthropogenic radiative forcings can be parameterized through the CO_2 forcing profile.

By a similar rationale, we have not considered the stochastic perturbations by volcanic events (note the highly uncertain radiative properties of each eruption, as discussed in Robock & Free 1995; see also Crowley, Cristie, & Smith 1993). If the two major volcanic sulfate forcings by eruptions of Krakatoa (1883; 6° south) and Katmai (1912; 58° north) can indeed be used to suggest fast ocean response time (and low overall climate sensitivity; Lindzen 1994), then the volcanic factor contributes primarily to short-term (interannual) global temperature variance over 1880–1993. Although we consider that forcings by volcanic and anthropogenic aerosols are smaller than the two forcings studied in this paper, they deserve consideration in future studies.

REFERENCES

Antonucci, E., Hoeksema, J. T., & Scherrer, P. H. 1990, ApJ, 360, 296
Arendt, S. 1992, ApJ, 389, 421
Baliunas, S. L., & Soon, W. H. 1995, ApJ, 450, 896
Bevington, P. R., & Robinson, D. K. 1992, Data Reduction and Error Analysis for the Physical Science (New York: McGraw-Hill)
Bracewell, R. N. 1988, MNRAS, 230, 535
Butler, C. J., & Johnston, D. J. 1994, Irish Astron. J., 21, 251
Cess, R. D., et al. 1993, Science, 262, 1252
Chapman, G. A., Cookson, A. M., & Dobias, J. J. 1994, ApJ, 432, 403
Charlson, R. J., Schwartz, S. E., Hales, J. M., Cess, R. D., Coakley, J. A., Jr., Hansen, J. E., & Hofmann, D. J. 1992, Science, 255, 423
Christy, J. R. 1995, Climatic Change, 31, 455
Cox, S. J., Wang, W. C., & Schwartz, S. E. 1995, Geophys. Res. Lett., 22, 2509

Crowley, T. J., Cristie, T. A., & Smith, N. R. 1993, Geophys. Res. Lett., 20, 209
Crowley, T. J., & Kim, K.-Y. 1996, Geophys. Res. Lett., 23, 359
Dicke, R. H. 1988, Sol. Phys., 115, 171
Endal, A. S., Sofia, S., & Twigg, L. W. 1985, ApJ, 290, 748
Erickson, D. J., III, Oglesby, R. J., & Marshall, S. 1995, Geophys. Res. Lett., 22, 2017
Fontenla, J., White, O. R., Fox, P. A., Avrett, E. H., Harvey, K. L., & Kurucz, R. L. 1995, Eos, 76, S234
Foukal, P., Harvey, K., & Hill, F. 1991, ApJ, 383, L89
Foukal, P., & Lean, J. 1990, Science, 247, 556
Friis-Christensen, E., & Lassen, K. 1991, Science, 254, 698
———. 1993, Two and a Half Centuries of Solar Activity Variations and a Possible Association with Global Temperature (Danish Meteorol. Inst. Sci. Rep. 93-4)
Gaffin, S. R., Hoffert, M. I., & Volk, T. 1986, J. Geophys. Res., 91, 3944
Ghil, M. 1991, in The Sun in Time, ed. C. P. Sonett, M. S. Giampapa, & M. S. Matthews (Tucson: Univ. Arizona Press), 511
Gilliland, R. L. 1982, ApJ, 253, 399
———. 1989, Palaeogeogr. Palaeoclimat. Palaeoecol., 75, 35
Gilliland, R. L., & Schneider, S. H. 1984, Nature, 310, 38
Gleissberg, W. 1944, Terr. Magn. Atmos. Electricity, 49, 243
Gough, D. O. 1988, in Solar-Terrestrial Relationships and the Earth Environment in the Last Millennia, ed. G. Cini Castagnoli (Amsterdam: North-Holland), 90
———. 1990, Philos. Trans. R. Soc. London A, 330, 627
Haigh, J. D. 1994, Nature, 370, 544
Hameed, S., & Gong, G. 1994, Geophys. Res. Lett., 21, 2693
Hansen, J., Johnson, D., Lacis, A., Lebedeff, S., Lee, P., Rind, D., & Russell, G. 1981, Science, 213, 957
Hansen, J., & Lebedeff, S. 1987, J. Geophys. Res. D, 92, 13345
———. 1988, Geophys. Res. Lett., 15, 323
Hasselmann, K. 1976, Tellus, 28, 473
Hoffert, M. I., Callegari, A. J., & Hsieh, C. T. 1980, J. Geophys. Res. C., 85, 6667
Hoffert, M. I., Frei, A., & Narayanan, V. K. 1988, Climatic Change, 13, 267
Hoyng, P. 1993, A&A, 272, 321
Hoyt, D. V., Kyle, H. L., Hickey, J. R., & Mashhoff, R. H. 1992, J. Geophys. Res., 97, 51
Hoyt, D. V., & Schatten, K. H. 1992, ApJ, 384, 361
———. 1993, J. Geophys. Res., 98, 18895
Kelly, P. M., & Wigley, T. M. L. 1992, Nature, 360, 328
Kiehl, J. T., & Briegleb, B. P. 1993, Science, 260, 311
Kim, H. H., & Huang, N. E. 1993, Newly Found Evidence of Sun-Climate Relationships (NASA Tech. Mem. 104583)
Kuhn, J. R., & Libbrecht, K. G. 1991, ApJ, 381, L35
Laskar, J., Joutel, F., & Boudin, F. 1993, A&A, 270, 522
Lassen, K., & Friis-Christensen, E. 1995, J. Atmos. Terr. Phys., 57, 835
Lean, J., Beer, J., & Bradley, R. 1995, Geophys. Res. Lett., 22, 3195
Lee, R. B., III, Gibson, M. A., Wilson, R. S., & Thomas, S. 1995, J. Geophys. Res., 100, 1667
Lindzen, R. S. 1994, Annu. Rev. Fluid Mech., 26, 353
Lindzen, R. S., & Farrell, B. 1980, Mon. Weather Rev., 108, 2064
Lockwood, G. W., Skiff, B. A., Baliunas, S. L., & Radick, R. R. 1992, Nature, 360, 653
Lorenz, E. N. 1990, Tellus, 42, 378
Nesme-Ribes, E., Ferreira, E. N., Sadourny, R., Treut, H. Le., & Li, Z. X. 1993, J. Geophys. Res., 98, 18923
Oliver, R., & Ballester, J. L. 1994, Sol. Phys., 152, 481
Parker, D. E., Jones, P. D., Folland, C. K., & Bevan, A. 1994, J. Geophys. Res., 99, 14373
Parker, E. N. 1995, ApJ, 440, 415
Peixoto, J. P., & Oort, A. H. 1992, Physics of Climate (New York: AIP)
Posmentier, E. S. 1990, Ann. Geophys., 8, 781
———. 1994, Nonlinear Processes Geophys., 1, 26
Reid, G. C. 1987, Nature, 329, 142
———. 1991, J. Geophys. Res., 96, 2835
Ribes, J. C., & Nesme-Ribes, E. 1993, A&A, 276, 549
Robock, A., & Free, M. P. 1995, J. Geophys. Res., 100, 11549
Schatten, K. H. 1996, ApJ, 460, L69
Schatten, K. H., & Orosz, J. A. 1990, Sol. Phys., 125, 179
Schlesinger, M. E., & Ramankutty, N. 1992, Nature, 360, 330
Shine, K. P., Derwent, R. G., Wuebbles, D. J., & Morcrette, J. J. 1990, in Climate Change: The IPCC Scientific Assessment, ed. J. T. Houghton, G. J. Jenkins, & J. J. Ephraums (New York: Cambridge Univ. Press), 41
Siegenthaler, U., & Sarmiento, J. L. 1993, Nature, 365, 119
Soon, W. H., Baliunas, S. L., & Zhang, Q. 1994, in The Solar Engine and Its Influence on Terrestrial Atmosphere and Climate, ed. E. Nesme-Ribes (NATO ASI Ser. I, 25) (Heidelberg: Springer), 133
Spruit, H. C. 1994, in The Solar Engine and Its Influence on Terrestrial Atmosphere and Climate, ed. E. Nesme-Ribes (NATO ASI Ser. I, 25) (Heidelberg: Springer), 102
Steinegger, M., Vázquez, M., Bonet, J. A., & Brandt, P. N. 1996, ApJ, 461, 478
Stone, P. H., & Risbey, J. S. 1990, Geophys. Res. Lett., 17, 2173
Swinson, D. B., Koyama, H., & Saito, T. 1986, Sol. Phys., 106, 35
Tang, F., Howard, R., & Adkins, J. M. 1984, Sol. Phys., 91, 75
Taylor, K. E., & Penner, J. E. 1994, Nature, 369, 734
Tinsley, B. A., Hoeksema, J. T., & Baker, D. N. 1994, J. Geophys. Res., 99, 16805
Verma, V. K. 1993, ApJ, 403, 797
Vizoso, G., & Ballester, J. L. 1990, A&A, 229, 540
Waldmeier, M. 1957, Z. Astrophys., 43, 149
———. 1961, The Sunspot Activity in the Years 1610–1960 (Zurich: Schulthess)
———. 1971, Sol. Phys., 20, 332
Wang, W. C., Dudek, M. P., & Liang, X. Z. 1992, Geophys. Res. Lett., 19, 1357
Willson, R. C., & Hudson, H. S. 1991, Nature, 351, 42
Yi, W. 1992, JRASC, 86, 89
Zhang, Q., Soon, W. H., Baliunas, S. L., Lockwood, G. W., Skiff, B. A., & Radick, R. R. 1994, ApJ, 427, L111